ELSEVIER

Journal of Structural Geology 28 (2006) 2204–2221

JOURNAL OF STRUCTURAL GEOLOGY

www.elsevier.com/locate/jsg

Fault-induced perturbed stress fields and associated tensile and compressive deformation at fault tips in the ice shell of Europa: implications for fault mechanics

Simon A. Kattenhorn*, Scott T. Marshall[1]

Department of Geological Sciences, University of Idaho, PO Box 443022, Moscow, ID 83844-3022, USA

Received 5 October 2004; received in revised form 2 September 2005; accepted 30 November 2005
Available online 26 January 2006

Abstract

Secondary fractures at the tips of strike-slip faults are common in the ice shell of Europa. Large magnitude perturbed stress fields must therefore be considered to be a viable driving mechanism for the development of part of the fracture sequence. Fault motions produce extensional and compressional quadrants around the fault tips. Theoretically, these quadrants can be associated with tensile and compressive deformational features (i.e. cracks and anti-cracks), respectively. Accordingly, we describe examples of both types of deformation at fault tips on Europa in the form of extensional tailcracks and compressional anti-cracks. The characteristics of these features with respect to the plane of the fault create a fingerprint for the mechanics of fault slip accumulation when compared with linear elastic fracture mechanics (LEFM) models of perturbed stress fields around fault tips. Tailcrack kink angles and curving geometry can be used to determine whether opening accompanies sliding motion. Kink angles in the 50–70° range are common along strike-slip faults that resemble ridges, and indicate that little to no opening accompanied sliding. In contrast, tailcrack kink angles are closer to 30° for strike-slip faults that resemble bands, with tailcrack curvatures opposite to ridge-like fault examples, indicating that these faults undergo significant dilation and infill during fault slip episodes. Anti-cracks, which may result from compression and volume reduction of porous near-surface ice, have geometries that further constrain fault motion history, corroborating the results of tailcrack analysis. The angular separation between anti-cracks and tailcracks are similar to LEFM predictions, indicating the absence of cohesive end-zones near the tips of Europan faults, hence suggesting homogeneous frictional properties along the fault length. Tailcrack analysis can be applied to the interpretation of cycloidal ridges: chains of arcuate cracks on Europa that are separated by sharp kinks called cusps. Cusp angles are reminiscent of tailcrack kink angles along ridge-like strike-slip faults. Cycloid growth in a temporally variable tidal stress field ultimately resolves shear stresses onto the near-tip region of a growing cycloid segment. Thus, resultant slip and associated tailcrack development may be the driving force behind the initiation of the succeeding arcuate segment, hence facilitating the ongoing propagation of the cycloid chain.

Keywords: Europa; Faults; Strike-slip; Tailcracks; Anti-cracks; Compression; Stress

1. Introduction

It has long been recognized that fractures of various types develop alongside terrestrial faults and intrusive dikes in response to motion along the fault or magma pressure within the dike (e.g. Delaney et al., 1986; Pollard, 1987; Rubin, 1993; Kattenhorn and Watkeys, 1995; Petit and Mattauer, 1995; Willemse et al., 1997; Vermilye and Scholz, 1998). Because these fractures are a direct result of the faulting or dike injection, they are referred to as secondary fractures, implying they would not have developed in the absence of the structure with which they are affiliated. The exact type of secondary fracture that develops will depend on the available stresses, fluid pressures, and rock properties, but may include joints,

* Corresponding author. Tel.: +208 885 5063; fax: +208 885 5724.
E-mail address: simkat@uidaho.edu (S.A. Kattenhorn).
[1] Current address: Department of Geological Sciences, 233 Morrill Science Center, University of Massachusetts, 611 North Pleasant Street, Amherst, MA 01003-9297, USA.

0191-8141/$ - see front matter © 2005 Elsevier Ltd. All rights reserved.
doi:10.1016/j.jsg.2005.11.010

veins, pressure solution surfaces, minor shear fractures, or even fully-developed faults or fault systems. In all cases, the secondary fractures form in response to the growth of the primary feature and may even facilitate further growth by providing a zone of weakness through which the primary feature can propagate.

Secondary fractures may develop in the form of macroscale tailcracks (or wing cracks) that emanate away from the tips of faults or slipping interfaces such as joints or bedding planes (Rispoli, 1981; Cruikshank et al., 1991; Cruikshank and Aydin, 1994; Petit and Mattauer, 1995; Willemse et al., 1997; Martel and Boger, 1998; Younes and Engelder, 1999; Cooke et al., 2000; Kattenhorn et al., 2000). All such slipping interfaces are hereafter referred to simply as faults. Tailcracks are extremely common tension fractures that form on opposite sides of opposite tips of a fault (where present at both tips), defining a pattern that is a direct indicator of the shear sense along the fault (Fig. 1a). Tailcracks may also develop at points along a fault where it deviates from planarity (such as at jogs, steps, and relay zones), or at points of variable frictional properties along the fault surface (Cooke, 1997). Tailcracks have very different orientations to the fault with which they are associated and are typically curved (Fig. 1b and c). Although tailcracks are usually smaller than the fault along which they formed, it is possible for them to reach lengths in excess of the primary feature when a large crack-parallel compression exists (Brace and Bombolakis, 1963; Erdogan and Sih, 1963; Hoek and Bieniawski, 1965; Nemat-Nasser and Horii, 1982).

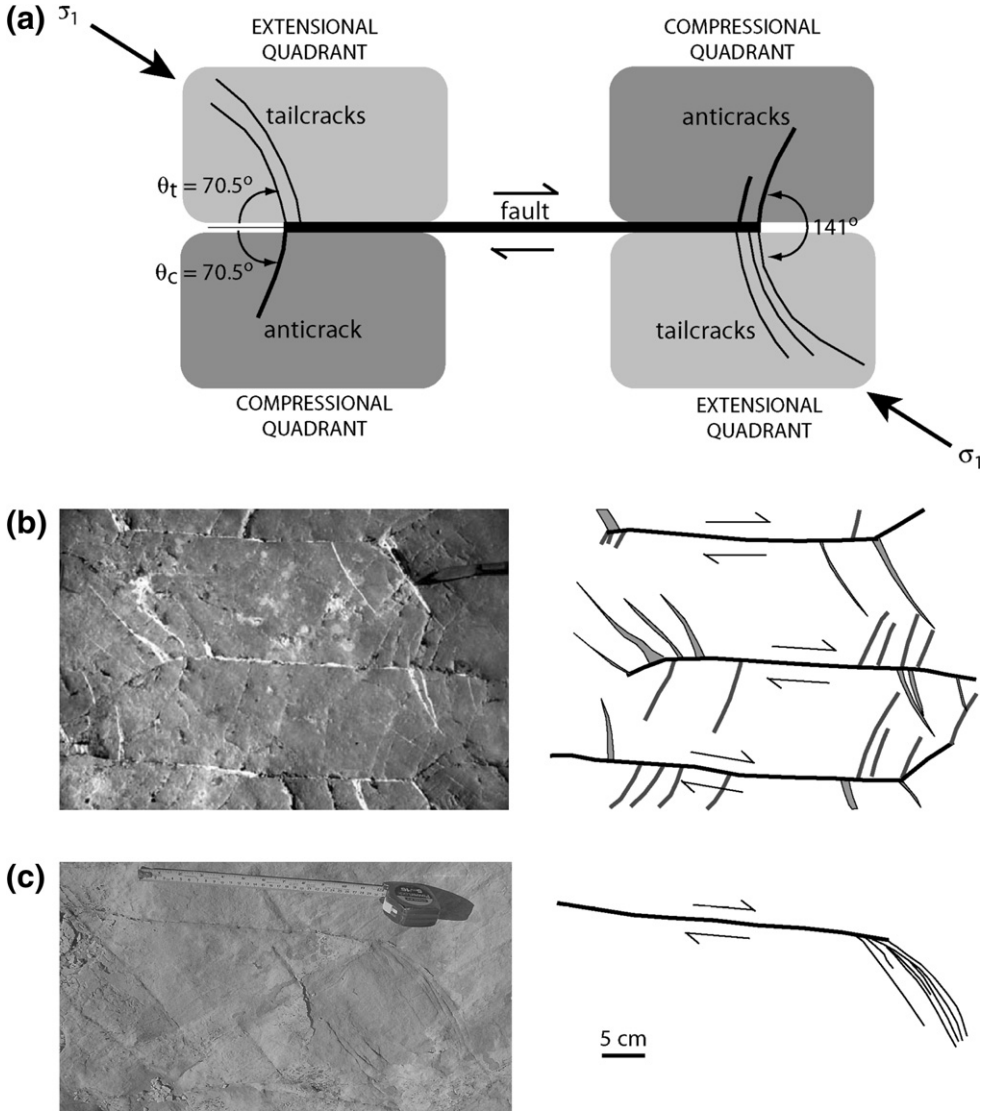

Fig. 1. (a) Schematic diagram showing the locations and orientations of tailcracks and anti-cracks that would form at the tips of a right-lateral strike-slip fault. The left-lateral case is the mirror image of this illustration. Extensional and compressional quadrants are antisymmetrically distributed about opposite fault tips. Tailcracks form in extensional quadrants with a kink angle, θ_t=70.5°. Anti-cracks form in compressional quadrants with a kink angle, θ_c=70.5°. The far-field maximum compressive stress direction is shown as σ_1. (b) Example of vein-filled tailcracks (light gray) and anti-cracks (dark gray) along right-lateral slipped fractures (black) in limestone at Languedoc, France. Knife blade for scale. (c) Example of tailcracks with an opposite sense of curvature to (b) at the tip of a right-lateral slipped joint in sandstone in Nevada, U.S.A. The total slip was a few millimeters.

The quantitative aspects of the mechanics of tailcrack development have been described in great detail in many previous works (Erdogan and Sih, 1963; Hussain et al., 1974; Sih, 1974; Cotterell and Rice, 1980; Pollard and Segall, 1987; Cruikshank et al., 1991; Willemse and Pollard, 1998) and so will not be repeated here. In essence, tailcracks are manifestations of brittle failure in response to high tensile stress magnitudes created at the tip of a fault. These stresses are theoretically infinite right at the fault tip; however, the finite strength of brittle materials always results in the development of cracks as soon as the stresses reach a value equal to the strength of the material (whether tensile or compressive). In response to the shear motion, the perturbed stress field at the tip of the fault is thus both greater in magnitude, and different in principal stress orientations, to the remote (far-field) stress that caused the fault to slip. As a result, tailcracks propagate away from the fault tip in a direction governed by the characteristics of the perturbed stress state, but always perpendicular to the direction of maximum tensile stress at the propagating tip of the tailcrack. The locations of tailcracks are governed by the locations of the regions of high tension (extensional quadrants) at the fault tips, which occur to one side of each tip with an antisymmetric pattern dependent on the slip sense (Fig. 1a). Mutually opposite sides of each tip zone experience a region of increased compression (compressional quadrants).

The junction between the tailcrack and the fault defines an angle called the kink angle (θ_t in Fig. 1a, where the subscript t stands for tensile), which in mathematical models of pure mode II motion (in fracture mechanics terminology), laboratory models, and field observations of many terrestrial faults is commonly about 70° (e.g. Pollard and Segall, 1987) when measured in a section plane that contains the slip vector along the fault. The kink angle decreases as the amount of fault opening increases, reaching 0° for the pure mode I case (Cruikshank et al., 1991; Willemse and Pollard, 1998), indicating that a tension crack will tend to propagate in its own plane. Deviations from this 70° angle have been observed in terrestrial examples (Granier, 1985; Cooke, 1997; Willemse et al., 1997; Martel and Boger, 1998; Younes and Engelder, 1999) and have been attributed to changes in driving stresses or the presence of a region of increased friction near the fault tip, called a cohesive end-zone (CEZ) (Martel, 1997; Martel and Boger, 1998; Willemse and Pollard, 1998).

As a tailcrack propagates away from a fault tip, it gradually moves from a region dominated by the perturbed stress field into one dominated by the remote stress field. This effect is a logical consequence of linear elastic fracture mechanics (LEFM) behavior, in which the magnitude of the perturbed stress field, normalized against the remote stress field, is controlled by the fault length and the stress drop. The perturbed field decays away from a fault tip as a function of the inverse of the square-root of the radial distance from the fault tip ($1/r^{1/2}$) when very near to the tip, and as a function of the inverse of the square of the radial distance from the fault center ($1/r^2$) at distances from the fault in excess of the fault length (Pollard and Segall, 1987; Lawn, 1993). The end result is that tailcracks grow with curved paths and only straighten out when entering the region dominated by the remote stress field or a region of spatially homogeneous stress orientations such as may exist within a relay zone between overlapping fault segments (Kattenhorn et al., 2000; Crider and Peacock, 2004). In the latter case, the tailcracks and other secondary fractures may facilitate hard linkages between the fault segments (e.g. Crider and Pollard, 1998). Tailcracks are thus extremely informative features in that they provide a fingerprint for the state of paleostress responsible for both fault motion and tailcrack growth.

A fault tip may also develop contractional features in the compressional quadrants to either side of the tips of a fault, commonly accompanying tailcracks in the extensional quadrants. These so-called anti-cracks (Fletcher and Pollard, 1981) form perpendicular to the maximum compressive stress direction (unlike tailcracks) and, as such, are also governed by the characteristics of the near-tip, fault-perturbed stress field. The most common form of anti-crack in terrestrial rocks is likely to be a solution surface, although compaction bands in sandstones that undergo a reduction of pore space (Antonellini et al., 1994) are another possibility. As might be expected, anti-cracks are most commonly described from rocks prone to pressure solution, such as carbonate rocks or rock salt (e.g. Rispoli, 1981; Petit and Mattauer, 1995; Willemse et al., 1997) (Fig. 1b), and have been interpreted to form with orientations that can be predicted using either LEFM or CEZ predictions of stress orientations in compressional quadrants (Fletcher and Pollard, 1981; Pollard and Segall, 1987; Willemse and Pollard, 1998). It should be noted that, for pure mode II motion (i.e. no opening along the shearing crack), the orientations of principal stresses in the compressional quadrants of the perturbed field predict kink angles for contractional features (θ_c in Fig. 1a, where the subscript c stands for compression) that are identical to those of tailcracks (i.e. 70.5°), resulting in a predicted 141° angle between tailcracks and solution surfaces that formed at the same fault tip in LEFM models (Fletcher and Pollard, 1981; Pollard and Segall, 1987) (Fig. 1a), in contrast to a predicted 90° angle in CEZ models (Willemse and Pollard, 1998). This angle between the tailcracks and anti-cracks increases as the mode II/mode I ratio decreases in LEFM models; however, an increasing mode I component of motion also results in a greatly reduced maximum compressive stress in the compressional quadrants (Willemse and Pollard, 1998), which may thus decrease the likelihood of the development of solution seams.

In this paper, we will demonstrate that secondary fractures are not only endemic to terrestrial faults but are also produced within perturbed stress fields associated with numerous faults in the ice shell of Jupiter's moon, Europa. We describe examples of clearly identifiable tailcracks at the tips of strike-slip faults on Europa and explain their usefulness in unraveling the mechanics of fault motions. We also show that some features at the tips of strike-slip faults are likely to be previously unrecognized anti-cracks that reflect the effects of compression and volume loss near the fault tip. We also hypothesize that curved and cuspate cracks on Europa, called cycloids, which contain kinked features called cusps that closely resemble tailcracks, may have undergone the same formational

mechanism. In each type of secondary fracturing process, we demonstrate the applicability of the LEFM approach in unraveling the mechanics of fracturing on Europa, analogous to the study of crustal fractures on Earth.

2. Stresses, fractures, and faults on Europa

2.1. Tidal stresses

Europa is the fourth largest of the Galilean satellites of Jupiter, having a diameter of 3122 km: only slightly smaller in size than Earth's moon. Europa is seemingly unique in the solar system in that it contains a 100–170-km-thick outer layer of water that overlies a silicate mantle and a metallic core (e.g. Anderson et al., 1998; Pappalardo et al., 1999; Schubert et al., 2004). The outermost portion of the water layer is solid ice of unknown exact thickness, but probably at least 1–30 km based on a variety of estimation techniques such as flexure analysis, thermodynamic models of convection, and impact models (see Billings and Kattenhorn (2005) for a comprehensive summary). Europa was extensively imaged by the Voyager and Galileo spacecraft missions, with Galileo images providing the best resolution of surface details at as little as tens of meters/pixel.

The ice shell is pervasively fractured (Fig. 2) in response to the continuous flexing and longitudinal oscillation of tidal bulges induced by the gravitational pull of Jupiter during each slightly elliptical Europan orbit. The resultant global tidal stresses are called diurnal stresses (Helfenstein and Parmentier, 1980, 1983; Greenberg et al., 1998; Hoppa et al., 1999a,b) which, at any point on Europa, vary in both magnitude and orientation throughout the Europan day, undergoing a constant counter-clockwise rotation in the northern hemisphere and clockwise rotation in the southern hemisphere. Maximum diurnal stress magnitudes are <100 kPa (Hoppa et al., 1999b; Crawford et al., 2005; Gleeson et al., 2005). In addition to the diurnal stress field, it has been hypothesized that Europa also experiences a long-term, faster-than-synchronous rotation of the ice shell with respect to the satellite interior, which causes a longitudinal migration of the tidal bulges over $>12{,}000$ years per rotation (Hoppa et al., 1999c, 2001). This reorientation of the tidal bulges induces a second component to the stress field termed the nonsynchronous rotation stress field (Helfenstein and Parmentier, 1985; McEwen, 1986; Geissler et al., 1998a; Greenberg et al., 1998). The magnitude of the nonsynchronous rotation stress is dependent on the amount of shell reorientation over which stresses are able to accumulate elastically (perhaps a few degrees), and is potentially an order of magnitude or more greater than diurnal stress magnitudes (Leith and McKinnon, 1996; Greenberg et al., 1998). Crawford et al. (2005) suggest that nonsynchronous rotation stresses are only able to swamp diurnal stress magnitudes if stresses are able to accumulate over about 10° of shell reorientation. Finally, any polar wander of the ice shell, although unconfirmed, would contribute an additional component of global stress (Ojakangas and Stevenson, 1989;

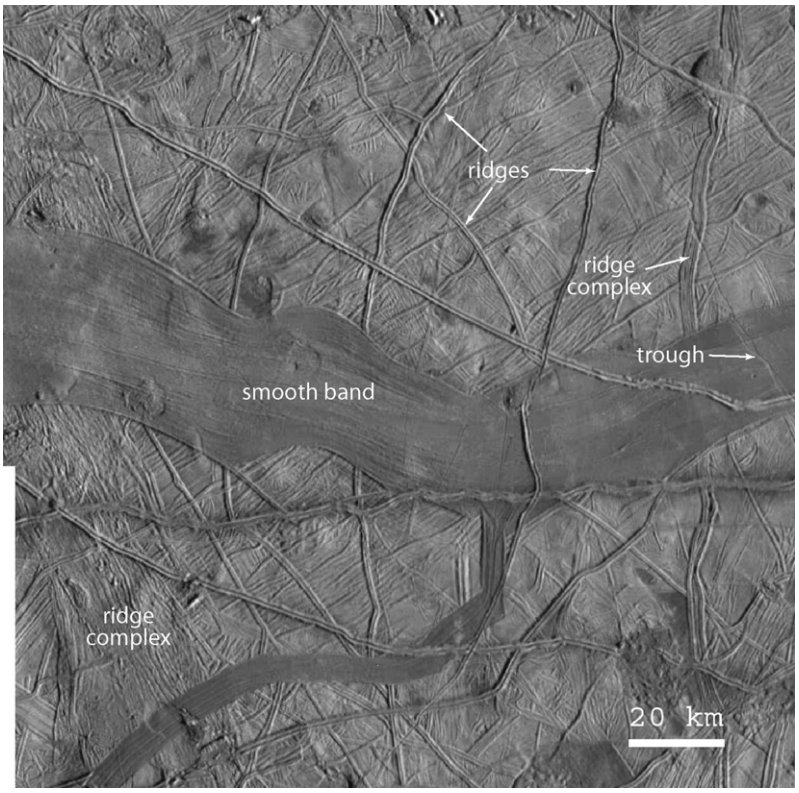

Fig. 2. Pervasively fractured ice shell of Europa, showing various fracture types as described in the main text. Galileo mosaic of a feature termed 'The Sickle,' taken during the E11 orbit.

Leith and McKinnon, 1996; Sarid et al., 2002). The combination of all sources of stress are likely responsible for the majority of the fracture patterns visible on the surface of Europa today, as well as the range of fracture morphologies that reflect different formational processes and evolutionary developments through the visible geologic history. Nonetheless, none of these sources of stress are able to produce stress magnitudes as high as those produced at the tip of a sliding or opening crack (i.e. perturbed stress fields), which would thus be the most effective at initiating new cracking.

2.2. Fracture types

The fractures in the ice shell of Europa span a wide range of orientations and morphologies (Fig. 2) that reflect a range of mechanical behaviors as the ice shell underwent brittle deformation. Based on a relatively low cratering density, the surface is believed to be geologically young, possibly as young as 30–70 Ma (Zahnle et al., 2003), in response to an effective resurfacing process by both tectonic and cryovolcanic mechanisms (Sullivan et al., 1998; Geissler, 1999; Figueredo and Greeley, 2004), with the latter being dominant in the most recent geologic history. Geologic mapping at scales ranging from pole-to-pole regional mapping (Prockter et al., 1999; Figueredo and Greeley, 2000, 2004) to local detailed mapping (Spaun et al., 1998; Kattenhorn, 2002) has revealed an identifiable fracture sequence compatible with the long-term effects of nonsynchronous rotation of the ice shell and associated changes in stress conditions over long time scales.

The range of fracture morphologies has led to a number of classification schemes for lineament types (Lucchitta and Soderblom, 1982; Geissler et al., 1998b; Greenberg et al., 1998; Pappalardo et al., 1998a; Head et al., 1999; Prockter et al., 1999; Figueredo and Greeley, 2000, 2004; Greeley et al., 2000; Kattenhorn, 2002). Despite small differences in terminologies among different works, it has generally been established that there are a small number of distinct types of fractures that can be observed almost everywhere on the Europan surface (Fig. 2). The most primitive (in terms of fracture development) and commonly the youngest type of fracture is called a trough, representing any open crack at the surface, regardless of the indeterminate depth of penetration into the ice shell, that does not exhibit raised rims along the flanks of the crack. Where raised rims occur along a fracture, it is termed a ridge (or double ridge), which represents the most common type of lineament on the surface. The exact origin of the ridges is still debated (Pappalardo et al., 1999; Kattenhorn, 2004b) but is likely to be the result of either extrusion of icy material pumped to the surface from the underlying ocean by tidal processes (i.e. a tension fracturing process; Geissler et al., 1998b; Greenberg et al., 1998), or warm ice that moved up to the surface in response to frictional shear heating along the crack walls, also driven by tidal effects (i.e. a shear fracturing process; Gaidos and Nimmo, 2000; Nimmo and Gaidos, 2002; Spaun et al., 2003).

At least two types of features appear to reflect larger-scale (up to 10s of km) crustal spreading processes in the ice shell. The first is a class of features called either complex ridges or ridge complexes (Fig. 2), which are comprised of numerous adjacent or anastomosing ridges (Head et al., 1999; Tufts et al., 2000; Figueredo and Greeley, 2004) that may represent a long period of spreading in a manner analogous to a dike swarm. The remaining crustal spreading features are called bands (Fig. 2), which exhibit a subdued upper surface commonly dissected by normal faults (Kattenhorn, 2002; Prockter et al., 2002; Figueredo and Greeley, 2004), and sometimes exhibiting bilateral symmetry about a central trough, prompting comparison with a mid-ocean spreading ridge development mechanism (Sullivan et al., 1998; Prockter et al., 2002). Although bands are a morphologically distinct class of Europan lineament, they likely represent an end-member in an evolutionary sequence of fracture development, beginning with troughs, then ridges, then either bands or ridge complexes, in response to tidal reworking of existing cracks in the ice shell (Geissler et al., 1998b; Greenberg et al., 1998; Pappalardo et al., 1998a; Tufts et al., 2000).

3. Strike-slip faults

3.1. General characteristics

Many lineaments also show clear evidence of lateral offsets of pre-existing fractures cut by the lineament, and are thus classified as strike-slip faults (Hoppa et al., 1999a, 2000; Tufts et al., 1999; Prockter et al., 2000; Sarid et al., 2002; Greenberg, 2004; Kattenhorn, 2004a). The morphologies of these strike-slip faults are variable but generally identical to the classes of fracture types described above. Kattenhorn (2004a) differentiates two main styles of faulting based on morphology: ridge-like and band-like, reflecting that some faults exhibit raised rims flanking a central trough, thus resembling ridges, whereas other faults morphologically resemble bands (Fig. 3).

Fault motions have been hypothesized to be driven by rotating diurnal tidal stresses that cause faults to experience a combination of opening and forward shear motion, followed by closing and a lesser amount of frictional backward shear motion. This cycle, referred to as tidal walking (Hoppa et al., 1999a), allows faults to accumulate displacement over time like a ratchet, and provides a plausible mechanism for fault activity driven by the tidal stress field. However, this model is not necessarily compatible with all fault slip sense characteristics on Europa (Kattenhorn, 2004a); it does not attempt to account for the range of visible fault morphologies, nor does it consider faults as finite fractures governed by physical laws in terms of slip behavior and related deformation such as secondary fracturing.

3.2. Tailcracks in extensional quadrants

Although there have been a number of studies describing strike-slip fault locations, orientations, sense of slip, and slip magnitude on Europa, only a few previous works have acknowledged secondary fracturing induced by perturbed stress fields during fault activity (Schenk and McKinnon, 1989; Prockter et al., 2000; Schulson, 2002; Kattenhorn, 2004a).

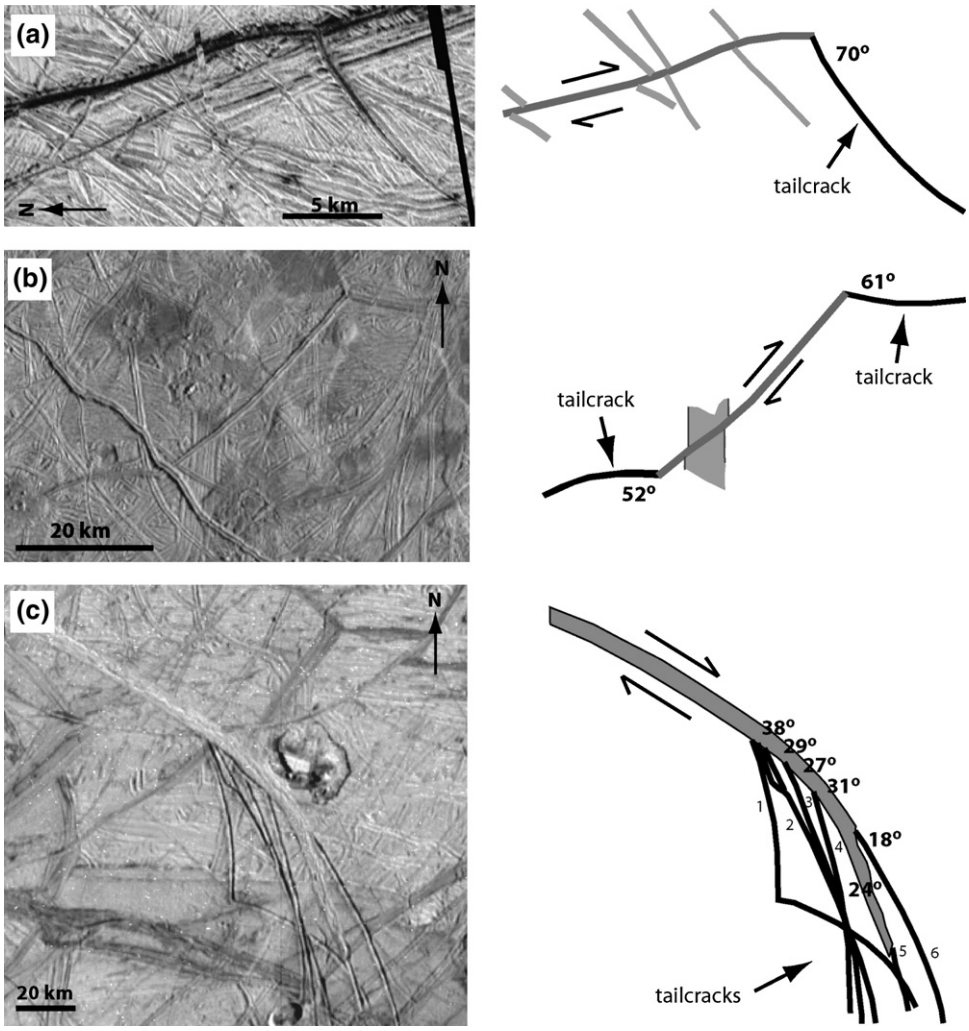

Fig. 3. Tailcracks associated with two different styles of strike-slip faulting: ridge-like ((a) and (b)) and band-like (c). Offset lineaments are shown where identifiable. (a) This 12-km-long tailcrack in Argadnel Regio (17.8°S, 196.7°W) formed a kink angle of 70° in the extensional quadrant of a ridge-like fault that underwent 600 m of right-lateral motion. Imaged during the E12 Galileo orbit. (b) A 40-km-long ridge-like fault near Conamara Chaos (12.5°S, 269°W). Tailcracks formed in the extensional quadrants at both tips in response to ~700 m of right-lateral offset. The kink angles and sense of curvature of the tailcracks are similar to those associated with other ridge-like faults. Imaged during the E6 orbit. (c) The eastern tip of Agenor Linea, a 1500-km-long band-like fault in Europa's southern hemisphere that formed a cluster of at least six tailcracks. Kink angles are much lower than ridge-like faults and the sense of curvature of tailcracks is comparatively reversed. The order of development of the tailcracks is numbered 1–6 and is based on crosscutting relationships (the timing of tailcrack 6 is uncertain). Imaged during the E17 orbit.

Consequently, there has been no direct comparison undertaken between terrestrial and Europan strike-slip fault mechanics. Those studies that have focused on the specifics of deformation at fault tips clearly demonstrate that the ice shell is deformed through secondary deformational processes. Nonetheless, the previous works that considered secondary fracturing were predominantly observational, not quantitative.

A rigorous analysis of tailcracks requires consideration of the mechanics of tailcrack development from a LEFM standpoint in order to identify the mechanical significance of secondary fracturing characteristics for fault slip behavior. Despite the theoretical prediction of 70° tailcracks for mode II cracks, which are commonly used to approximate the behavior of terrestrial strike-slip faults, tailcrack angles on Europa vary widely, from 30 to 80° in a survey by Kattenhorn (2004a). Nonetheless, the distribution of tailcrack angles is not random, but rather varies with strike-slip fault morphology. In almost all cases, high-angle tailcracks (resembling mode II predictions) are associated with ridge-like faults, which show a median tailcrack angle of 53°, whereas lower angle tailcracks are associated with band-like faults, which have a median tailcrack angle of only 30°. Since tailcrack angles are controlled by the characteristics of the perturbed stress field which, in turn, are dictated by the specifics of the relative motions of the fault walls, the marked discrepancy in tailcrack characteristics between these two fault styles that are morphologically different is likely a reflection of mechanical differences in fault slip accumulation behavior.

To examine these differences, in Fig. 3 we show examples of fault-tip tailcracks associated with three right-lateral

strike-slip faults on Europa. In each case, the amount and sense of motion is discernible along the fault and is always compatible with the tailcracks having formed in the extensional quadrant of each respective fault. In Fig. 3a, a 12-km-long tailcrack formed at almost exactly 70° to the 23-km-long ridge-like fault that underwent a maximum of 600 m of right-lateral motion, creating a fracture geometry analogous to the predictions of pure mode II cracks (Fig. 1a). The tailcrack curves away from the intersection point with the fault in a manner again analogous to tailcracks along theoretical mode II faults. In Fig. 3b, a 40-km-long, slightly curved ridge-like fault has undergone about 700 m of right-lateral offset, resulting in the development of tailcracks at both tips of the fault. In this example, the tailcracks appear to intersect the fault at slightly smaller angles compared with Fig. 3a, forming kink angles of 61 and 52°, respectively. As with Fig. 3a, both tailcracks curve away from the fault tips towards an orientation presumably indicative of a far-field stress orientation just beyond the influence of the perturbed stress field at the tips.

In contrast to the two ridge-like fault examples, the strike-slip fault in Fig. 3c is a band-like fault. The image shows a 140-km-wide region at the eastern end of Agenor Linea, a ~1500-km-long prominent bright band in Europa's southern hemisphere that has undergone up to 20 km of right-lateral offset (Prockter et al., 2000). Where this offset dies out at the eastern tip, a cluster of at least six tailcracks has developed in the extensional quadrant of the fault tip, analogous to horsetails (arrays of multiple tailcracks at a single fault tip) along terrestrial strike-slip faults. However, each tailcrack formed at significantly smaller angles to the fault than the examples associated with ridge-like faults. Tailcrack angles here vary from 18 to 38°, with seemingly decreasing kink angles with increasing proximity to the current fault tip. Based on cross-cutting relationships between individual tailcracks, the order of development of the tailcracks, numbered 1–6 in Fig. 3c, also migrates towards the current fault tip, suggesting that older tailcracks formed when the fault tip existed at points progressively further west moving backwards through time. The fault has begun utilizing tailcrack 5 to facilitate continued growth. The tailcracks curve away from the fault tip with a sense of curvature that is the opposite to that of tailcracks along ridge-like faults (Fig. 3a and b). Such tailcrack characteristics are common along band-like faults.

3.3. Anti-cracks in compressional quadrants

Sarid et al. (2002) and Greenberg (2004) describe regions of lateral convergence and potential crustal recycling associated with strike-slip faults. Although they provided no explicit physical mechanism for the manifestation of the convergence or an analysis of the geometric relationships between faults and associated contractional features, they were the first to present evidence of such fault-related features. The zones of contraction are described as being band-like with internal striations similar to dilational bands, but with edges that do not match each other and which cannot be reconstructed, unlike typical dilational bands, producing an overall appearance reminiscent of muscle tissue. In each of the examples they describe, the hypothesized contraction features occur in what we determine to have been the compressional quadrant of each respective fault, based on the sense of fault slip.

The search for evidence of contraction and crustal removal has been crucial to the understanding of the tectonics of the ice shell because the abundant dilational features and associated creation of new crust cannot be reconciled with a non-expanding shell unless an equal amount of surface area is somehow removed and recycled into the interior. Nonetheless, regions of contractional strain have been elusive, comprising of rare examples of a gentle crenulation of the ice shell (Prockter and Pappalardo, 2000). It has also been suggested that compression of regions of disaggregated crust called chaos may have been able to accommodate adjacent crustal extension (Greenberg et al., 1999), although the initial formation of chaos is likely in response to thermodynamic recycling through endogenetic diapirism (Pappalardo et al., 1998b; McKinnon, 1999; Collins et al., 2000; Schenk and Pappalardo, 2002).

We now present evidence to demonstrate that crustal contraction sites can be mechanically linked to motions along strike-slip faults and their associated, quantifiable perturbed stress fields. We therefore treat these features as anti-cracks, using the terrestrial terminology applied to the development of solution surfaces, as described earlier. Furthermore, the contraction features, which occur within the compressional quadrants of faults, may accompany secondary tensile fractures such as tailcracks that develop within the extensional quadrants of the same faults. Taken together, we will show how such features provide important clues to the mechanical behavior and growth history of strike-slip faults.

In Fig. 4a, we show a 290 km by 322 km region of Argadnel Regio (commonly referred to as the Wedges region), which contains numerous right-lateral strike-slip faults and associated dark bands that formed by dilation and intrusive infill of tailcracks that developed at the fault tips (Schenk and McKinnon, 1989; Schulson, 2002; Kattenhorn, 2004a). These features will simply be referred to as tailcracks here despite their ultimate development into dark bands, analogous to the vein-filled tailcracks in limestone in Fig. 1b. The locations of strike-slip faults and associated tailcracks are shown in Fig. 4b, as well as tailcrack kink angles. In each example, the tailcrack occurs on the predicted extensional quadrant side of the fault tip, based on the sense of fault offset. The two northernmost fault segments have similar E–W strike orientations but the southernmost segment is oriented NW–SE. Tailcrack kink angles are measured at the exact location where the fault and tailcrack intersect, taking into consideration the local fault and tailcrack orientations at these junction points. The kink angles vary across a wide range, from 29 to 80°. Only the southernmost tailcrack, which has the highest kink angle, has a triangular shape and a definable tip; all other tailcracks are tabular and facilitated linkage between adjacent fault segments.

Close examination of the compressional quadrant sides of each tip reveals another class of secondary features (Fig. 4c)

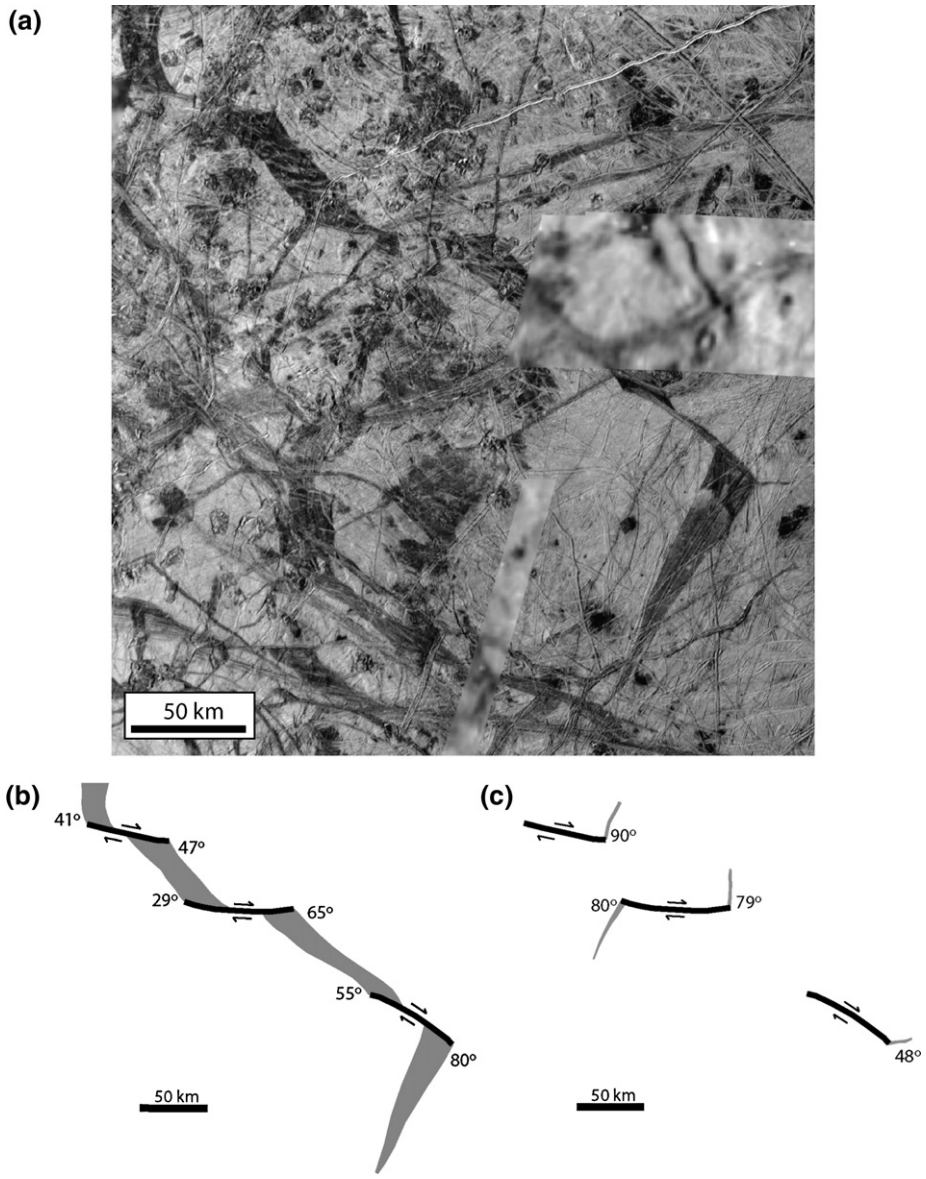

Fig. 4. (a) A region of Argadnel Regio, or 'Wedges,' as imaged during the E14 orbit. The region is dissected by numerous right-lateral strike-slip faults that have caused dilation and the formation of bands. Small portions of the fault zone are only imaged in low resolution, as shown. Image mosaic: NASA/JPL/PIRL, U. Arizona. (b) Locations of three prominent faults and associated tailcracks in the extensional quadrants. All tailcracks have been dilated and infilled to form bands, some of which have facilitated the linkage of fault segments. Kink angles are variable and are discussed in the text. (c) Fault segments as in (b) and associated locations of compressional quadrant anti-cracks.

that resemble infilled tailcracks in that they are triangular with identifiable tips and form dark band-like material; however, they are both shorter and narrower than the dilated tailcrack bands. We deduce that these bands in the compressional quadrants are likely to represent contractional features, or anti-cracks, that helped accommodate the near-tip contractional strain associated with motion along the faults. The anti-crack kink angles vary from 48 to 90°, with the southernmost fault exhibiting the lowest kink angle. The other three identifiable anti-cracks define kink angles in the 79–90° range. A comparison of Fig. 4b and c reveals that the tailcracks and anti-cracks define contrasting kink angles at corresponding fault tips. The angle between the tailcracks and anti-cracks (separation angle) at specific fault tips varies from 113 to 144°, with three of the four examples exhibiting angles greater than 128°.

In order to justify the supposition that these secondary fractures are tailcracks and anti-cracks, some of the more readily identifiable lineaments affected by the middle fault segment in Fig. 4 are mapped onto a reprojected spacecraft image in Fig. 5a. The fault is 80 km long and has undergone about 27 km of right-lateral offset, based on piercing points. The region is structurally complex and records a long history of tectonic events that have resulted in numerous superimposed and crosscutting lineaments. The faulting itself is likely to be relatively old, evidenced by a large number of post-faulting deformation events that have deformed the

tailcrack bands and crosscut the fault with younger ridges. Furthermore, the entire region has been disrupted by the development of lenticulae (e.g. Spaun et al., 2002), which are the small, rounded pit features that create a mottled effect to the surface and are likely related to geologically recent diapirism. Nonetheless, it is possible to match features to either side of the fault as well as across the dilated tailcracks, consequently indicating that the opening vectors are different in the two tailcracks (Fig. 5a).

A structural reconstruction of offset features along the fault (Fig. 5b) is complicated by the fact that the fault trace is not perfectly linear and the motion vectors are slightly different at each end of the fault, which has likely impacted on the slip history and associated deformation. Nonetheless, features can be matched up perfectly by reconstructing the effects of dilation along the tailcracks, whereas it is not possible to perfectly reconstruct features in the compressional quadrants. Gaps in the reconstructed image (white regions in Fig. 5b)

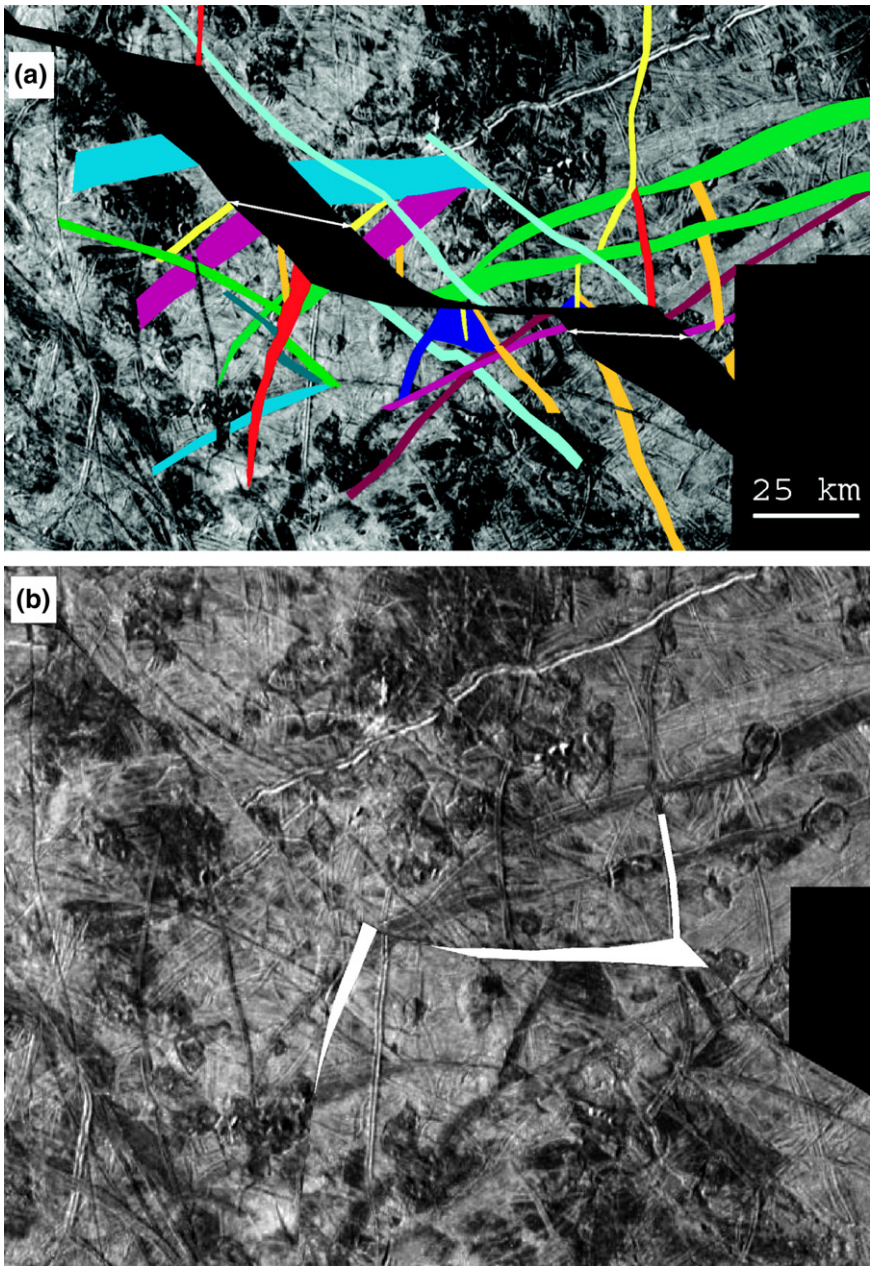

Fig. 5. (a) Geologic map of the middle fault in Fig. 4 showing major lineaments affected by 27 km of right-lateral offset. All features younger than the faulting are ignored. The fault zone and associated dilation is shown in black. Contractional features are shown in red. Dilation vectors for each tailcrack are shown with white double-headed arrows and indicate differences in fault motion vectors between the eastern and western ends of the fault. (b) Structural reconstruction of the offset features shown in (a). Features can be matched across the fault almost perfectly by un-dilating the tailcracks; however, in the reconstructed image, portions of crust appear to be missing in the compressional quadrants of the fault and along the eastern half of the fault trace (regions shown in white). These regions were greatly compressed and perhaps partially subsumed by contractional deformation in zones of fault-induced compression and are thus no longer visibly intact at the surface, instead appearing as dark anti-cracks.

appear to demarcate zones of missing crust in the region of the hypothesized anti-cracks, particularly at the western tip. Analogous missing crust along other reconstructed faults is described by Sarid et al. (2002) and Greenberg (2004). These gaps are likely to be recording locations where parts of the surface were either highly compressed or absorbed into the ice shell and recycled into the interior. Some of the missing material was consumed along the eastern part of the fault itself (white region along the fault in Fig. 5b), presumably in response to the bend in the fault trace and resultant compression along the eastern part of the fault in response to the motion vector further west being oblique to the eastern portion of the fault (as evidenced by tailcrack opening vectors in Fig. 5a).

Although the anti-cracks somewhat resemble the convergence bands described by Sarid et al. (2002), consisting of a dark, finely lineated material, the walls of the anti-cracks are more distinct in the examples described here. This apparent difference may represent the effects of either different stress conditions or different physical processes by which material is consumed (e.g. collapse of pore space in the ice versus contractional deformation through faulting or folding).

3.4. The LEFM perspective

The characteristics of the tailcracks and anti-cracks described above can be placed into the context of LEFM models of perturbed stress fields at the tips of sliding faults. As described in Section 1, the geometries of secondary fractures can be explicitly predicted using LEFM theoretical models, and have proven accurate in accounting for terrestrial examples of secondary fracturing. Pure mode II cracks that lack cohesive end-zones are predicted to develop tailcracks and anti-cracks that both form with ~70° kink angles, thus defining a separation angle ($\theta_t+\theta_c$ in Fig. 1a) of ~140°. However, as the ratio of mode I to mode II loading varies, so also do the respective kink angles of tailcracks (θ_t) and anti-cracks (θ_c). Similar changes in kink angles may be associated with the presence of a cohesive end-zone near the fault tip; however, as explained by Willemse and Pollard (1998), the separation angle between extensional and compressional quadrant features to either side of a particular fault tip remains constant at 90° in all mixed-mode CEZ models, regardless of loading conditions, whereas LEFM solutions predict that the separation angle increases from 140° towards 180° as the ratio of mode I to mode II loading increases (i.e. as more opening accompanies slip).

In the Europan tailcrack and anti-crack examples presented here, the separation angle is never 90°; rather, it is always closer to the 140° prediction for LEFM cracks, strongly suggesting that cohesive end-zone models are not appropriate for ice faults on Europa. This result is supported by laboratory measurements of low frictional properties of ice at low temperatures (Rist et al., 1994), which perhaps imply a low likelihood of a zone of high friction near a fault tip.

In order to evaluate the implications of secondary fracturing along Europan strike-slip faults for the mechanics of fault motions, it is important to look at both the kink angles as well as the broader-scale geometry of secondary fractures as they propagated within the perturbed stress field away from the fault tip. In Fig. 6, we show the characteristics of the LEFM perturbed stress field (calculated using the equations in Segall and Pollard (1987)) along the right half of a right-lateral fault, for three loading conditions: mode I/mode II ratios of 0 (no opening), 1, and 2, respectively, represented as ratios of stress intensity factors, K_I and K_{II}. In each example, we also show the predicted geometries of both tailcracks and anti-cracks that have the potential to form at the fault tip.

For the pure mode II case (Fig. 6a), tailcracks and anti-cracks have identical 70° kink angles; however, as the amount of opening that accompanies shear motion increases, the kink angle of tailcracks decreases whereas the kink angle of anti-cracks increases. Correspondingly, the separation angle between the two types of features increases slightly from 140 to 147° (Willemse and Pollard, 1998). In response to the effects of the characteristics of the perturbed stress field as K_I/K_{II} increases, tailcrack curvature becomes less pronounced, with the tailcrack tending towards being more in-plane with the fault as it propagates away from the fault tip, and even possibly undergoing a reversal in the sense of curvature (with respect to the mode II case) as it propagates

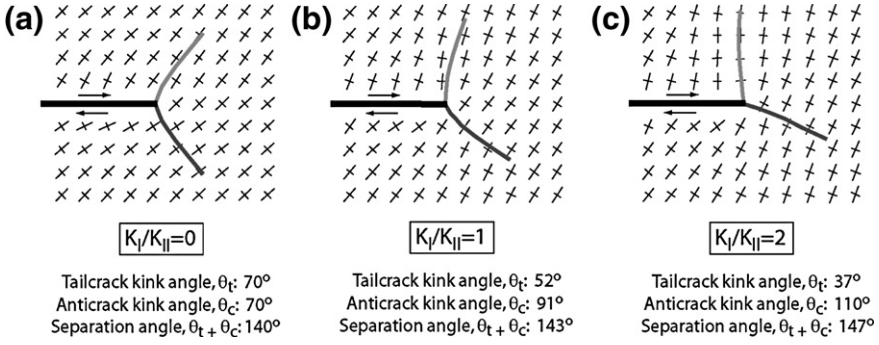

Fig. 6. Characteristics of the perturbed stress field along the right half of a right-lateral fault (black), calculated using LEFM solutions (Pollard and Segall, 1987). Long ticks represent the maximum tensile stress directions, whereas short ticks represent the maximum compressive stresses. Three loading conditions are shown, represented as ratios of stress intensity factors, K_I and K_{II}: (a) mode I/mode II ratio of 0 (i.e. pure mode II; no opening). (b) Mode I/mode II ratio of 1. (c) Mode I/mode II ratio of 2. In each example, the predicted geometries of both tailcracks (dark gray) and anti-cracks (light gray) are shown at the fault tip, with kink angles listed below each scenario (using the same conventions as Fig. 1a) as determined from Willemse and Pollard (1998).

out into the ambient remote stress field for $K_I/K_{II} \approx 2$. In contrast, anti-cracks become less curved with increasing mode I component, forming almost perpendicular to the trend of the fault in the range $K_I/K_{II}=1-2$ (Fig. 6b and c).

These results can be applied to secondary fractures along Europan strike-slip faults to highlight the mechanics of fault development and to corroborate the deduction that the band-like features in the compressional quadrants of the faults in Fig. 4 are examples of contraction features, or anti-cracks. Firstly, as described in detail by Kattenhorn (2004a), the fact that ridge-like faults have high median tailcrack angles (53°) compared with band-like faults (30°; Fig. 3) suggests that the mode of fault slip differs between these two fault types. Many ridge-like faults exhibit tailcracks angles of about 70° (Fig. 3a), suggesting pure mode II slip (Fig. 6a). Where the kink angles are slightly less (Fig. 3b), it can be concluded that either a small amount of opening accompanied fault motion or that the nature of the kink angle at the junction between the fault and tailcrack is not fully resolvable at the resolution of the spacecraft images. Nonetheless, the geometry of ridge-like tailcracks, in terms of both kink angle and sense of tailcrack curvature, closely resembles many terrestrial examples (Fig. 1b) as well as the theoretical predictions in the range of loading conditions exhibited in Fig. 6a and b.

In contrast, tailcracks along band-like faults (Fig. 3c) do not resemble typical tailcrack geometries along large terrestrial strike-slip faults or the theoretical predictions for mode II cracks, but rather more closely resemble the theoretical predictions shown in Fig. 6c in which the opening component of loading exceeds the shear component. Under these circumstances, the fault walls are likely to separate during fault motion, allowing ice to rise from an underlying source (whether a liquid ocean or ductile ice) to produce new crustal material, hence explaining the band-like appearance. Furthermore, tailcracks growing at the fault tips form low kink angles (or even gentle veers), and curve in an opposite sense to tailcracks along ridge-like faults. A terrestrial centimeter-scale geometric analog is shown in Fig. 1c, in which a cluster of tailcracks occurs along a slipped joint in sandstone. The decrease in kink angles in successively younger tailcracks with increasing proximity to the present tip of Agenor Linea (Fig. 3c) reflects an increasing K_I/K_{II} ratio for younger tailcracks, probably reflecting a greater amount of opening along the fault in response to a change in its strike orientation as it grew (becoming progressively more southerly).

In cases where anti-cracks in the compressional quadrants at fault tips occur in conjunction with tailcracks in the extensional quadrants (true of all the examples described here; Figs. 4 and 5), the characteristics of the two types of features can be used in combination to deduce details of the mechanical evolution of the fault. In Fig. 4, the southernmost fault segment exhibits different tailcrack and anti-crack configurations to the northern two segments, as well as differing in fault strike. If fault motion on all three segments was driven by a similar far-field driving stress (taking into account that tidal stresses are spatially variable over fairly large distances), it would be expected that the far-field stresses would cumulatively resolve differently onto the southernmost segment compared with the two northern segments, perhaps explaining differences in secondary fracturing geometries. The differently oriented faults may also have been active at different times. The high tailcrack angle (80°) on the southern segment implies no opening during fault motion (Fig. 6a), although the anti-crack angle (48°) is anomalously low (when compared with the 70° angle in Fig. 6a). One possible explanation is that the fault experienced a greater amount of fault-normal compression and fault-parallel tension than a pure mode II crack, which would be compatible with a lower anti-crack kink angle and a greater-than-70° tailcrack kink angle. As long as the coefficient of ice friction is low, even a small amount of resolved shear may still induce fault slip in this scenario.

The stress field would have resolved differently onto the E–W oriented northern two segments in Fig. 4, possibly inducing some amount of fault opening. The tailcrack and anti-crack shapes and kink angles suggest a mechanical scenario somewhere in the range between Fig. 6a and b ($K_I/K_{II}<1$). The northernmost segment (tailcrack angles, θ_t, of 41 and 47°, anti-crack angle, θ_c, of 90°) more closely resembles Fig. 6b (theoretical $\theta_t=52°$; $\theta_c=91°$), whereas the middle segment ($\theta_t=65°$; $\theta_c=79$ and 80°) is a closer match to the pure mode II case in Fig. 6a ($\theta_t=70°$; $\theta_c=70°$). This explanation is compatible with the reconstruction of fault motions, which shows remnant opening along the northernmost fault segment after all lateral motions are reconstructed (top left corner of Fig. 5b), whereas the middle segment exhibits missing surface material, implying that the fault surfaces were in compressive contact, ultimately leading to contraction along the fault. The tailcrack band kink angle (29°) at the west tip of the middle segment is unusually low, although this geometry may be somewhat affected by the non-linearity of the fault trace as well as the fact that an older lineament trend appears to parallel the dilational bands (Fig. 5) and so could potentially have been utilized as pre-existing planes of weakness during tailcrack development.

4. Cycloidal ridges

Cycloidal ridges, also called cycloids or flexūs, are prominent arcuate cracks arranged into chains that may span many hundreds of kilometers in the form of repeating curved segments linked at sharp cusps (Fig. 7). They are common everywhere on Europa and crosscut most other lineaments, making them some of the geologically most recently formed fractures in the ice shell (Lucchitta and Soderblom, 1982; Figueredo and Greeley, 2000, 2004). Recent studies of cycloids generally agree that these features likely grew as tension cracks within the rotating diurnal stress field (Hoppa et al., 1999b, 2001; Bart et al., 2003; Marshall and Kattenhorn, 2004). The crack grows perpendicular to the rotating maximum tensile principal stress direction. As a result, the sense of curvature of a cycloid depends on both the hemisphere in which it grew as well as the direction of growth. For example, in the northern hemisphere, the counter-clockwise rotation of the diurnal principal stresses would cause an eastward-propagating cycloid to be concave

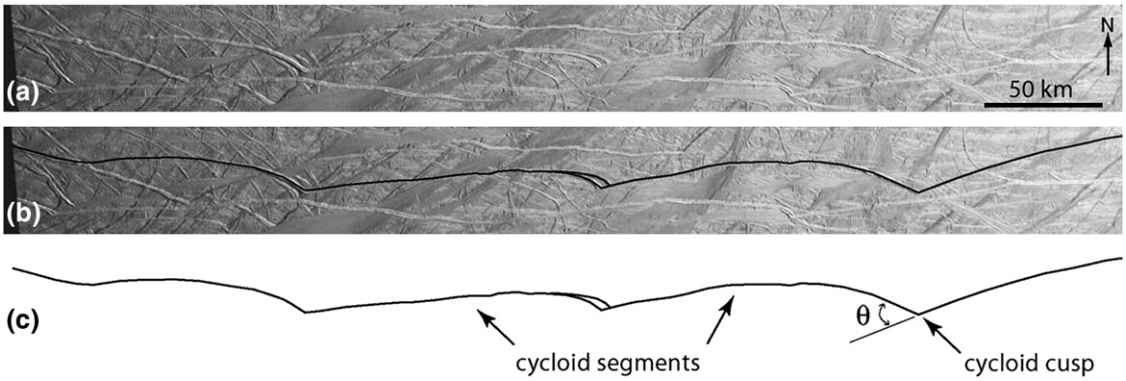

Fig. 7. (a) Example of a cycloid chain near 60°S in Europa's trailing hemisphere (from E17REGMAP01). (b) A trace over the cycloid ridges emphasizes the arcuate nature of the cycloids and regularity of joined segments. (c) Trace map showing definitions of cycloid segments, cusps, and cusp angle, θ.

towards the north, whereas a westward-propagating cycloid would be concave towards the south.

The sole model currently used to describe the details of cycloid propagation was developed by Hoppa et al. (1999b). In their model, cycloids are initiated when the maximum tensile principal stress exceeds the tensile strength of the ice shell, which is assumed to be very low (~40 kPa), and continue to grow as long as the tidal stresses exceed the crack propagation stress (which is smaller than the tensile strength). The cracks follow the rotating stress direction with a propagation velocity of ~3 km/hr, tracing out a curved fracture path until a point is reached in the orbit of Europa around Jupiter where the tidal stresses fall to a value below the crack propagation stress, at which time growth ceases. During a subsequent orbit, the process begins again; however, due to a difference in the maximum tensile principal stress direction between the time at which growth ceases and the time at which growth is re-initiated, a new cycloid segment forms with an initial crack orientation that differs from the end-point orientation of the previously formed segment, resulting in a sharp cusp between the two segments. This process can be self-repeating over many diurnal cycles, resulting in long chains of cycloid segments. Note that in this model, cycloid growth is always driven by a tensile stress associated with the diurnal tidal field.

In a survey of 112 cycloid cusp angles (θ in Fig. 7), we have found that although there is no characteristic cusp angle (we measured a range from 22 to 87°), cusps exhibit a high median angle of 58° with cusp angles skewed towards higher values (Marshall and Kattenhorn, 2005). This result is very similar to the median tailcrack kink angle measured along ridge-like strike-slip faults on Europa, as described in Section 3.4. Furthermore, cycloid cusps bear a marked morphologic resemblance to tailcracks (Fig. 8a), forming a sharp kink, and including a new fracture that grew in a curved manner away from an existing fracture. Although most cycloid cusps have a simple geometry involving the junction of two cycloid segments, there are also examples of cusps that exhibit a more complex geometry (Fig. 8b and middle cusp in Fig. 7), containing multiple ridge-like cracks that emanate from a single cycloid segment in the vicinity of the cusp, and which then generally coalesce into a single, new cycloid segment. These complex cusps have been observed to have as many as five splays, closely resembling horsetails that form along terrestrial faults as multiple tailcracks in an extensional quadrant.

Based on these observations, we suggest that cycloid cusps are in fact manifestations of a tailcracking process at the tip of a pre-existing cycloid segment that underwent shearing. This possibility is not difficult to justify considering the nature of the rotating diurnal stress field that produces the curved crack geometries (Fig. 9a) and causes any existing cycloid segment tip to necessarily experience constantly changing normal and shear stresses throughout each diurnal cycle. Based on the orientation of the maximum compressive stress, σ_1, at the instant of cusp development (indicated by the direction towards which the newly formed cycloid segment propagates away from the cusp in Fig. 9b), the principal stresses must have resolved shear stress onto the existing cycloid segment with a sense of shear that is always compatible with the new cycloid segment having formed as a tailcrack in the extensional quadrant of the shearing crack (Fig. 9c). If the coefficient of friction of Europan ice is low, and considering the evidence presented above for the lack of a cohesive end-zone near the tips of faults, even a small amount of shear stress is likely to drive sliding motion along the existing cycloid segment, which would result in a greatly magnified perturbed stress field at the segment tip (i.e. far in excess of the tidal stress magnitudes). Thus, it is the perturbed stress field, not the diurnal tensile stress, which likely induces the development of a new cycloid segment in the form of a tailcrack that initially propagates within the near-tip field but becomes dominated by the lower magnitude, far-field diurnal stresses with increasing distance from the cusp. The magnitude of the perturbed stress field at some distance from the tip of the sheared cycloid is governed by the length of the sliding portion of the cycloid (i.e. the crack length) and the available shear stress, but decays to ~3% in excess of the background value within two crack lengths away from the tip (Marshall and Kattenhorn, 2005). The tailcrack model for cycloid initiation circumvents the requirement of a low tensile strength (<0.04 MPa) of the ice, as suggested by Hoppa et al. (1999b), in order to initiate new crack growth by tidal stresses alone.

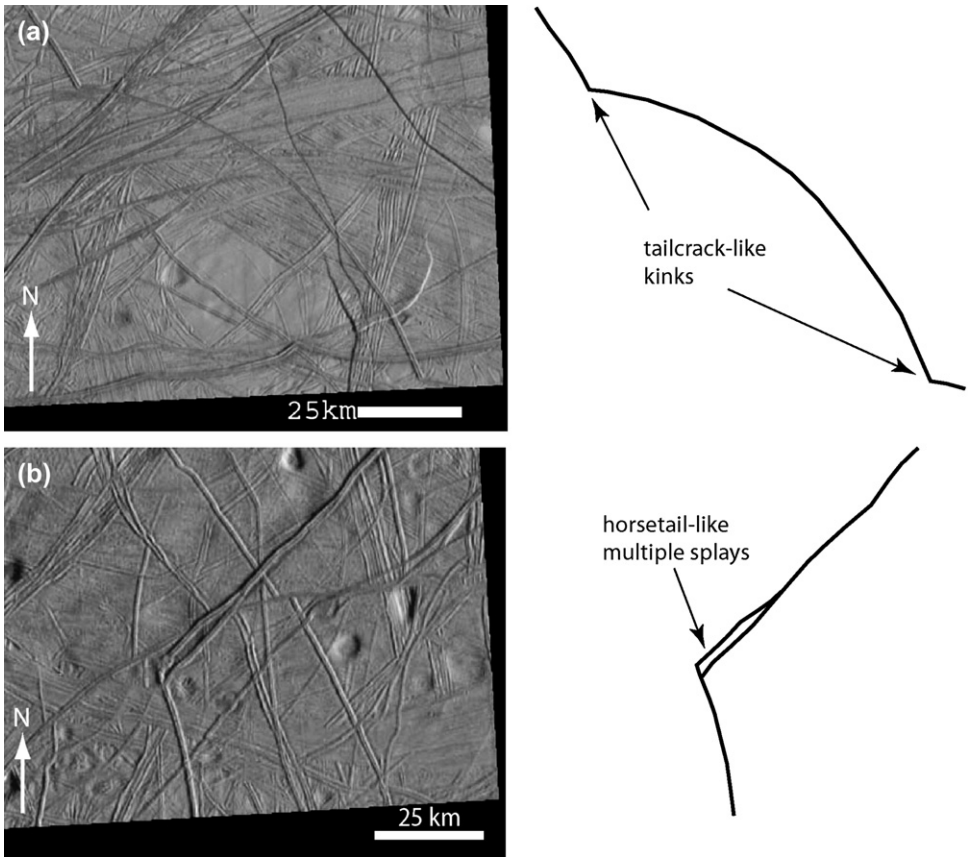

Fig. 8. Examples of cycloid cusps along cycloids imaged during the E15 orbit. (a) Simple cusps, each with a single tailcrack-like kink. (b) Complex cusp showing a double-kink resembling a tailcrack cluster or horsetail.

One caveat to the proposed mechanism for cusp formation is that shearing of the older segment should produce offsets of crosscut features along the cycloid trace. Such offsets are rarely observed, which we ascribe to the seemingly young age of cycloids, the mechanical difficulty for highly curved cracks to develop into prominent strike-slip faults, and the fact that, in LEFM theory, only a small amount of motion is needed to induce tailcracking which, at the limited resolution of Galileo images (typically 100s of meters per pixel), may be difficult or impossible to resolve. Furthermore, the sense of shear should reverse in this region near the cycloid segment tip during parts of the diurnal cycle yet tailcrack directions are always consistent at each cusp. This apparent conundrum may simply be a result of changing diurnal stress magnitudes during the diurnal cycle, only inducing shearing at peak magnitudes; however, a rigorous quantitative analysis is needed to fully characterize cusp development.

A comparison between cusp characteristics (Fig. 8) and LEFM solutions to the perturbed stress field at the tip of a mixed-mode crack (Fig. 6) suggests that the average cycloid undergoes a small amount of dilation at the instant of cusp/tailcrack development. This result is compatible with predictions of commonly tensile diurnal stresses which we hypothesize would cause opening of an existing cycloid during concomitant shearing. Nonetheless, the exact mechanics of motion along an existing cycloid would depend on the specifics of the diurnal stress field (which is both spatially and temporally variable; Greenberg et al., 1998) in the vicinity of the developing cusp, perhaps explaining the range of observed cusp angles, analogous to Europan strike-slip faults. Crawford et al. (2005) suggest that modification of the diurnal stress field by nonsynchronous rotation stresses may also affect cusp angles. Variable loading conditions between different cycloids in different locations, but which are nonetheless self-similar along an individual cycloid during recurring diurnal cycles, might be expected to result in morphological differences between cycloids (depending on whether dilation or shearing dominates; i.e. the ratio of K_I/K_{II} in Fig. 6). Accordingly, cycloids do appear to exhibit morphological variability, with some being distinctly trough- or ridge-like (>75% of all cycloids) and others resembling dilational bands (Marshall and Kattenhorn, 2005).

5. Discussion

Although previously published lineament formation models for Europa typically invoke the combined effects of diurnal tidal stresses and nonsynchronous rotation stresses to explain their development and orientations, such models fail to account for the possibility that some lineaments may develop in perturbed stress fields around slipping cracks. Although the majority of lineaments on Europa are undoubtedly related

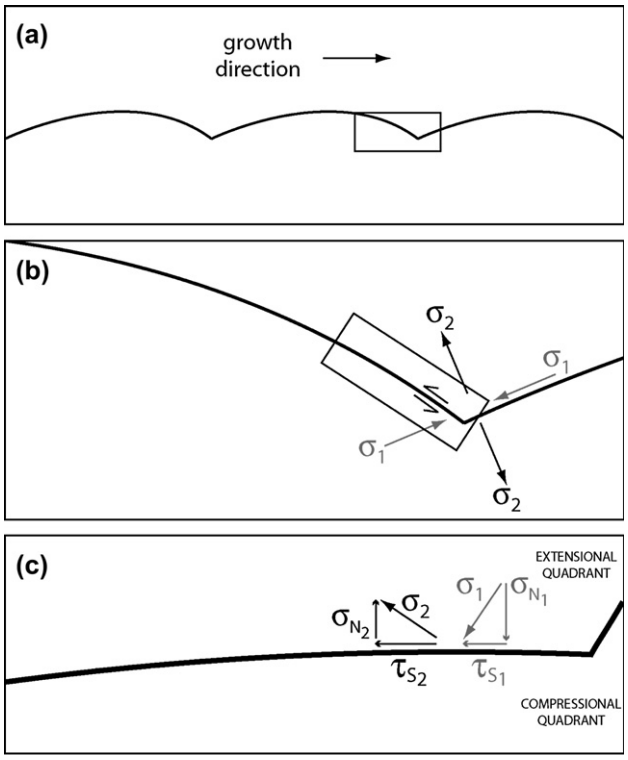

Fig. 9. Hypothetical example of a cycloid chain with stresses along the existing cycloid segment near a developing cusp, as resolved from the rotating diurnal stress field at the instant in time when the new cycloid segment starts to grow at the cusp. (a) Cycloid chain with boxed region of interest. (b) Orientations of principal tidal stresses. Actual magnitudes and orientations of tidal stresses are temporally variable at the diurnal time scale at this location and are spatially variable across all locations on Europa. (c) Resolved normal (σ_{N1} and σ_{N2}) and shear (τ_{s1} and τ_{s2}) components of stress, showing a net left-lateral shear stress that would drive tailcrack development in the extensional quadrant, in agreement with the growth direction of the new cycloid segment.

to some regional driving mechanism such as tidal stresses, we have demonstrated that secondary fracturing is relatively common and so should be considered to be a viable formation mechanism when developing a fracture sequence interpretation for any region of Europa. In fact, until fractures potentially heal through some form of ice annealing process within the ice crust, low frictional properties along the multitude of pre-existing cracks at any point in time should make shear or dilational reactivation by tidal stresses a relatively common process on Europa. The exact mode of reactivation (defined by the K_I/K_{II} ratio) should be both spatially and temporally variable due to the complex nature of the tidal stresses. Nonetheless, both dilational bands and strike-slip faults are common on Europa, highlighting the prevalence of both mode I and mode II deformation mechanisms.

Perturbed stress fields represent the perturbation to the ambient stress field induced by the relative motions of the walls of a crack. The nature of the perturbation is controlled by the specifics of these crack motions (Fig. 6). Very near to the tip of the slipping crack, perturbed stress magnitudes are many times higher than the driving stresses that induce crack motion in the first place, thus allowing secondary fractures to develop at the tip. This process is common along terrestrial faults in the form of tailcracks (in extensional quadrants) and anti-cracks or solution surfaces (in compressional quadrants), the orientations of which can be explained using LEFM theory. Along Europan strike-slip faults, tailcrack locations are always consistent with the sense of slip along the fault; however, tailcrack kink angles are variable. An examination of fault morphology as a function of median tailcrack kink angle reveals that where faults resemble ridges, tailcracks resemble the predictions for mode II cracks or mixed-mode I–II cracks with low K_I/K_{II} ratios (<1). Conversely, where faults resemble bands, tailcracks are more akin to mixed-mode I–II solutions where K_I/K_{II} is higher, possibly >2. In response, band-like fault tailcracks have an opposite sense of curvature to ridge-like fault tailcracks. These contrasting results highlight important differences in the evolution of morphologically different strike-slip faults on Europa. Most significantly, the tailcrack geometries indicate that opening along band-like faults must be concomitant with fault shear motion, as is advocated in the tidal walking mechanism (Hoppa et al., 1999a). In other words, band-like faults do not represent old lineaments that were dilated at some later point in time, as appears to be the case for most dilational bands, but rather represent a distinct style of fracture evolution on Europa. As such, band-like faults do not appear to have a terrestrial faulting analog because stresses on Earth are typically compressive and fault surfaces remain in contact in response to the effects of increasing lithostatic stresses with increasing depth (e.g. Crider and Pollard, 1998; Kattenhorn and Pollard, 1999).

Tailcrack geometries can also be used to unravel fault evolution in cases where dilation *was* a later event. Band-like faults that exhibit tailcracks that are more analogous to ridge-like fault tailcracks may have undergone a multi-phase evolution involving both mode II development (during which time the tailcrack developed) and a temporally separate dilational phase. This scenario is likely to have occurred along the southernmost fault segment in Fig. 4, which currently is band-like in appearance but which contains secondary fracturing indicators of non-dilational shear motion during fault slip.

LEFM models are also appropriate to explain the presence of secondary fractures in the compressional quadrants of strike-slip faults. These features somewhat resemble tailcracks and so may be mistakenly interpreted as being dilational features that formed at a time when a fault presumably underwent an opposite slip sense to that recorded by the present cumulative offset. For example, in Fig. 4c, the secondary cracks could be taken to represent the effects of ancient left-lateral motion along the faults even though all current offset indicators record many kilometers of right-lateral motion. However, all of these secondary fractures define distinctly different kink angles to the well-developed tailcracks in the current extensional quadrants of the faults. Furthermore, a structural reconstruction along the central segment (Fig. 5) suggests missing material was consumed along the compressional quadrant secondary fractures. The combination of these lines of evidence supports an anti-crack mode of development for these secondary fractures, indicating sites of contraction and removal of surface

area, as hypothesized along other Europan fault examples by Sarid et al. (2002) and Greenberg (2004). The exact nature of this volume loss is unclear. No thrust faulting is evident, and near-surface pressure solution is unlikely at the very low surface temperatures on Europa (~110 K) suggesting that the volume loss may be driven by some other process such as pore space reduction in the ice (cf. Eluszkiewicz, 2004), perhaps aided by ductile flow mechanisms at greater depths if the strain rates are sufficiently low. Antonellini et al. (1994) indicate that the porosity of terrestrial compaction bands may be as much as an order of magnitude less than the original porosity; hence, porosity reduction may be an efficient mechanism to reduce material volume.

The examples presented here provide the first mechanically based evidence that removal of portions of the ice crust, necessitated by the creation of wide expanses of new crustal material along dilational bands, is partially accommodated by motions along strike-slip faults and associated contraction in the compressional quadrants defined by the near-tip perturbed stress field. The effectiveness of this process to account for the removal of large amounts of surface area remains to be determined. In the anti-crack examples in Fig. 4, the maximum width of removed surface material is not likely to exceed about 5 km whereas 27 km of new material developed within the dilating tailcracks, resulting in a net surplus of new surface area.

The combination of tailcrack and anti-crack geometries in Fig. 4 can be used to unravel details of the mechanical behavior of the three fault segments. Individual kink angles strongly suggest minimal dilation accompanied slip along the fault surfaces. Furthermore, angles between tailcracks and anti-cracks at the same fault tip are close to the 140° angle predicted by LEFM models, and are never equal to the 90° angle predicted by CEZ models, implying that the frictional properties of ice faults on Europa do not change towards the fault tips, but are likely to be homogeneous along the fault length and possibly relatively insignificant.

Low frictional strength would permit relatively effective shear reactivation of unhealed fracture surfaces, even under high normal stress conditions. Cycloids are among the youngest fractures on the Europan surface and developed in a diurnal tide-dominated stress field that promoted arcuate crack growth. The rotating stress field must resolve both normal and shear stresses at the tip of an earlier formed cycloid segment at the instant of cusp development (Fig. 9), which, under low frictional strength conditions, would promote sliding and the creation of a mode-II-dominant perturbed stress field at the tip. Cusps between individual cycloid segments are morphologically similar to tailcrack kinks and display almost identical median kink angles to ridge-like strike-slip faults. It is thus not unreasonable to conclude a similar formational mechanism for these features, implying that the development of a cycloidal ridge chain is as much driven by the effects of perturbed stress fields associated with sheared cycloid segments as it is by the rotating diurnal principal stresses. Furthermore, high perturbed stress magnitudes at the tip of a propagating arcuate cycloid segment also obviate the suggested problem that diurnal stress magnitudes are too small to initiate cracking of the ice shell. Thus, criticism of the Hoppa et al. (1999b) model based on insufficient stress magnitude arguments should be considered moot.

6. Conclusions

Similarities between strike-slip faults on Earth and Europa are most pronounced when comparing the nature of secondary fractures generated at fault tips in response to motions along the fault. Strike-slip faults occur on Europa with great frequency; however, their morphologies are somewhat variable. In general, the faults can be divided into those that resemble ridges (ridge-like) and those that have undergone some amount of dilation and infill and thus resemble bands (band-like). Nonetheless, all types of strike-slip faults include numerous examples that exhibit secondary fractures at their tips, indicating that fault-perturbed stress fields are an important process for the generation of fractures on Europa.

Most secondary fractures occur in the form of tailcracks, which are tension fractures that parallel the trend of the spatially variable maximum compressive stress direction of the perturbed stress field on the extensional quadrant side of a fault tip. The tailcracks thus curve away from the fault tip, ultimately attaining an orientation dictated by the characteristics of the ambient far-field tidal stresses beyond the region of dominant influence by the perturbed stress field. An important difference exists between the characteristics of tailcracks at the tips of ridge-like faults and those at the tips of band-like faults. Ridge-like faults exhibit higher median tailcrack angles than those produced by band-like faults and curve away from the fault tip in a manner very analogous to many terrestrial tailcracks. Furthermore, the sense of curvature is typically relatively reversed along band-like fault tailcracks.

The strong similarity between Europan and terrestrial tailcracks suggests that a linear fracture mechanics (LEFM) analysis of their geometries is justified. Numerical models of variable styles of strike-slip fault mechanical behavior, ranging from pure mode II (no opening) to mixed-mode I–II (concomitant sliding and opening) for various ratios of mode I to mode II stress intensity (K_I/K_{II}), show marked differences in tailcrack shape and kink angle as the fault loading varies. Faults with surfaces that remain in contact during sliding (mode II) develop tailcracks with 70° kink angles; however, this angle decreases towards 52° as K_I approaches K_{II}. This range of results is compatible with the tailcracks observed along ridge-like faults, suggesting that these faults either remain closed during sliding or undergo a small amount of opening. When K_I exceeds twice the value of K_{II}, opening becomes dominant during fault motion and tailcracks form with angles closer to 30° and with a sense of curvature that may be opposite to instances where K_I/K_{II} is lower. These results are consistent with the characteristics of band-like fault tailcracks, indicating that band-like faults undergo dilation during slip rather than representing faults that were dilated long after their initial development. The faults are thus infilled with new crustal material from below while slip is accruing. Ridge-like and

band-like faults thus represent distinctly different mechanical styles of faulting.

Our examination of compressional quadrants of strike-slip faults in Argadnel Regio indicates that contractional strain may also be manifested in response to perturbed stress fields at fault tips in the form of compressional features we term anti-cracks. The exact nature of this deformation is unclear, but may involve some form of ice pore space collapse and volume reduction process, similar to compaction bands in terrestrial rocks. As such, these anti-cracks, like tailcracks, are good indicators of the characteristics of the perturbed stress field and reveal important details about the mechanics of fault motions. In particular, tailcracks and anti-cracks that form to either side of the same fault tip are separated by an angle approaching 140°, as is predicted by LEFM models but not predicted by models that assume the existence of a cohesive end-zone (CEZ) near the fault tip. Thus, the Europan faults examined are unlikely to exhibit a zone of increased friction near the fault tip, suggesting that friction is relatively homogeneous along the fault length. The existence of anti-cracks with predictable orientations at fault tips also provides the first theoretically justifiable evidence that zones of contraction may exist at fault tips that may partially accommodate the creation of new spreading-related surface area on Europa by allowing material to be consumed within zones of high compression in the perturbed stress field at a fault tip.

The success of LEFM models for unraveling details of secondary fracturing at fault tips may have other applications on Europa, particularly in terms of attempting to explain other features that could potentially represent secondary fracturing phenomena. For example, cycloids are prominent, geologically recent fractures on Europa that consist of arcuate fracture segments joined at kinked cusps. The cusps have geometries that resemble tailcracks, suggesting that a similar process of sliding and tailcrack growth may be integral to the cycloid growth process. The nature of the rotating diurnal principal stresses physically requires that shear stresses resolve onto pre-existing cycloid fracture segments during the Europan orbit around Jupiter. We conclude that these shear stresses, combined with the evidence for the lack of a cohesive zone near the fault tip, will likely initiate sliding, thus producing a highly magnified perturbed stress field at the cycloid segment tip in which a tailcrack develops to then initiate the continued growth of the cycloid chain. This model provides a mechanically plausible mechanism for the initiation of each curved cycloid segment, the full extent of which is driven by the rotating tidal stresses as described by Hoppa et al. (1999b).

Acknowledgements

This material is based upon work supported by the National Aeronautics and Space Administration under Grant No. NAG5-11495 issued though the Office of Space Science. Galileo images were reprojected using the ISIS program developed by the USGS. LEFM results were computed using a Mathematica script developed by Juliet Crider. The photograph in Fig. 1b was obtained from the Geo-FracNet website of Montpellier University, France (http://www.dstu.univ-montp2.fr/geofracnet/home.html). We thank an anonymous reviewer and Francis Nimmo for their helpful comments. Thanks also to Bob Pappalardo and Francis Nimmo for insightful discussions.

References

Anderson, J.D., Schubert, G., Jacobson, R.A., Lau, E.L., Moore, W.B., Sjogren, W.L., 1998. Europa's differentiated internal structure: inferences from four Galileo encounters. Science 281, 2019–2022.

Antonellini, M.A., Aydin, A., Pollard, D.D., 1994. Microstructure of deformation bands in porous sandstones at Arches National Park, Utah. Journal of Structural Geology 16, 941–959.

Bart, G.D., Greenberg, R., Hoppa, G.V., 2003. Cycloids and wedges: global patterns from tidal stress on Europa. Proceedings of the Lunar and Planetary Science Conference 34, 1396.

Billings, S.E., Kattenhorn, S.A., 2005. The great thickness debate: ice shell thickness models for Europa and comparisons with estimates based on flexure at ridges. Icarus 177, 397–412.

Brace, W.F., Bombolakis, E.G., 1963. A note on brittle crack growth in compression. Journal of Geophysical Research 68, 3709–3713.

Collins, G.C., Head, J.W., Pappalardo, R.T., Spaun, N.A., 2000. Evaluation of models for the formation of chaotic terrain on Europa. Journal of Geophysical Research 105, 1709–1716.

Cooke, M.L., 1997. Fracture localization along faults with spatially varying friction. Journal of Geophysical Research 102, 22,425–22,434.

Cooke, M., Mollema, P., Pollard, D.D., Aydin, A., 2000. Interlayer slip and fracture clusters within East Kaibab monocline: numerical analysis and field investigations. In: Cosgrove, J., Ameen, M. (Eds.), Drape Folds and Associated Fractures. Geological Society of London Special Publication 169, pp. 23–49.

Cotterell, B., Rice, J.R., 1980. Slightly curved or kinked cracks. International Journal of Fracture 16, 155–169.

Crawford, Z., Pappalardo, R.T., Barr, A.C., Gleeson, D., Mullen, M., Nimmo, F., Stempel, M.M., Wahr, J., 2005. Wavy lineaments on Europa: fracture propagation into combined nonsynchronous and diurnal stress fields. Proceedings of the Lunar and Planetary Science Conference 36, 2042.

Crider, J.G., Peacock, D.C.P., 2004. Initiation of brittle faults in the upper crust: a review of field observations. Journal of Structural Geology 26, 691–707.

Crider, J.G., Pollard, D.D., 1998. Fault linkage: three-dimensional mechanical interaction between echelon normal faults. Journal of Geophysical Research 103, 24,373–24,391.

Cruikshank, K.M., Aydin, A., 1994. Role of fracture localization in arch formation, Arches National Park, Utah. Geological Society of America Bulletin 106, 879–891.

Cruikshank, K.M., Zhao, G., Johnson, A.M., 1991. Analysis of minor fractures associated with joints and faulted joints. Journal of Structural Geology 13, 865–886.

Delaney, P.T., Pollard, D.D., Ziony, J.I., McKee, E.H., 1986. Field relations between dikes and joints: emplacement processes and paleostress analysis. Journal of Geophysical Research 91, 4920–4938.

Eluszkiewicz, J., 2004. Assessing porosity structure in Europa's crust. In: Workshop on Europa's Icy Shell: Past, Present, and Future, LPI Contribution No. 1195, Lunar and Planetary Institute, Houston, p. 27.

Erdogan, F., Sih, G.H., 1963. On the crack extension in plates under plane loading and transverse shear. Journal of Basic Engineering 85, 519–527.

Figueredo, P.H., Greeley, R., 2000. Geologic mapping of the northern leading hemisphere of Europa from Galileo solid-state imaging data. Journal of Geophysical Research 105, 22,629–22,646.

Figueredo, P.H., Greeley, R., 2004. Resurfacing history of Europa from pole-to-pole geological mapping. Icarus 167, 287–312.

Fletcher, R.C., Pollard, D.D., 1981. Anti-crack model for pressure solution surfaces. Geology 9, 419–424.

Gaidos, E.J., Nimmo, F., 2000. Tectonics and water on Europa. Nature 405, 637.
Geissler, P.E., 1999. Cryovolcanism in the outer solar system. In: Sigurdsson, H. (Ed.), Encyclopedia of Volcanoes. Academic Press, San Diego, pp. 785–800.
Geissler, P.E., Greenberg, R., Hoppa, G., et al., 1998. Evidence for non-synchronous rotation of Europa. Nature 391, 368–370.
Geissler, P.E., Greenberg, R., Hoppa, G., et al., 1998. Evolution of lineaments on Europa: clues from Galileo multispectral imaging observations. Icarus 135, 107–126.
Gleeson, D., Crawford, Z., Barr, A.C., Mullen, M., Pappalardo, R.T., Prockter, L.M., Stempel, M.M., Wahr, J., 2005. Wavy and cycloidal lineament formation on Europa from combined diurnal and nonsynchronous stress. Proceedings of the Lunar and Planetary Science Conference 36, 2364.
Granier, T., 1985. Origin, damping, and pattern of development of faults in granite. Tectonics 4, 721–737.
Greeley, R., Figueredo, P.H., Williams, D.A., et al., 2000. Geologic mapping of Europa. Journal of Geophysical Research 105, 22,559–22,578.
Greenberg, R., 2004. The evil twin of Agenor: tectonic convergence on Europa. Icarus 167, 313–319.
Greenberg, R., Geissler, P., Hoppa, G., Tufts, B.R., Durda, D.D., Pappalardo, R., Head, J.W., Greeley, R., Sullivan, R., Carr, M.H., 1998. Tectonic processes on Europa: tidal stresses, mechanical response, and visible features. Icarus 135, 64–78.
Greenberg, R., Hoppa, G.V., Tufts, B.R., Geissler, P., Riley, J., Kadel, S., 1999. Chaos on Europa. Icarus 141, 263–286.
Head, J.W., Pappalardo, R.T., Sullivan, R., 1999. Europa: morphological characteristics of ridges and triple bands from Galileo data (E4 and E6) and assessment of a linear diapirism model. Journal of Geophysical Research 104, 24,223–24,236.
Helfenstein, P., Parmentier, E.M., 1980. Fractures on Europa: possible response of an ice crust to tidal deformation. Proceedings of the Lunar and Planetary Science Conference 11, 1987–1998.
Helfenstein, P., Parmentier, E.M., 1983. Patterns of fracture and tidal stresses on Europa. Icarus 53, 415–430.
Helfenstein, P., Parmentier, E.M., 1985. Patterns of fracture and tidal stresses due to nonsynchronous rotation: implications for fracturing on Europa. Icarus 61, 175–184.
Hoek, E., Bieniawski, Z.T., 1965. Brittle fracture propagation in rock under compression. International Journal of Fracture Mechanics 1, 137–155.
Hoppa, G., Tufts, B.R., Greenberg, R., Geissler, P., 1999. Strike-slip faults on Europa: global shear patterns driven by tidal stress. Icarus 141, 287–298.
Hoppa, G.V., Tufts, B.R., Greenberg, R., Geissler, P.E., 1999. Formation of cycloidal features on Europa. Science 285, 1899–1902.
Hoppa, G.V., Greenberg, R., Geissler, P., Tufts, B.R., Plassman, J., Durda, D.D., 1999. Rotation of Europa: constraints from terminator and limb positions. Icarus 137, 341–347.
Hoppa, G., Greenberg, R., Tufts, B.R., Geissler, P., Phillips, C., Milazzo, M., 2000. Distribution of strike-slip faults on Europa. Journal of Geophysical Research 105, 22,617–22,627.
Hoppa, G.V., Tufts, B.R., Greenberg, R., Hurford, T.A., O'Brien, D.P., Geissler, P.E., 2001. Europa's rate of rotation derived from the tectonic sequence in the Astypalaea region. Icarus 153, 208–213.
Hussain, M.A., Pu, S.L., Underwood, J.H., 1974. Strain energy release rate for a crack under combined mode I and mode II. In: Fracture Analysis. Proceedings of the 1973 National Symposium on Fracture Mechanics II. American Society of Testing Materials Special Technical Publication 560, pp. 2–28.
Kattenhorn, S.A., 2002. Nonsynchronous rotation evidence and fracture history in the Bright Plains region, Europa. Icarus 157, 490–506.
Kattenhorn, S.A., 2004a. Strike-slip fault evolution on Europa: evidence from tailcrack geometries. Icarus 172, 582–602.
Kattenhorn, S.A., 2004b. What is (and isn't) wrong with both the tension and shear failure models for the formation of lineae on Europa. In: Workshop on Europa's Icy Shell: Past, Present, and Future. LPI Contribution No. 1195, Lunar and Planetary Institute, Houston, pp. 38–39.
Kattenhorn, S.A., Pollard, D.D., 1999. Is lithostatic loading important for the slip behavior and evolution of normal faults in the Earth's crust? Journal of Geophysical Research 104, 28,879–28,898.
Kattenhorn, S.A., Watkeys, M.K., 1995. Blunt-ended dyke segments. Journal of Structural Geology 17, 1535–1542.
Kattenhorn, S.A., Aydin, A., Pollard, D.D., 2000. Joints at high angles to normal fault strike: an explanation using 3-D numerical models of fault-perturbed stress fields. Journal of Structural Geology 22, 1–23.
Lawn, B., 1993. Fracture of Brittle Solids. Cambridge University Press, Cambridge. 378p.
Leith, A.C., McKinnon, W.B., 1996. Is there evidence for polar wander on Europa? Icarus 120, 387–398.
Lucchitta, B.K., Soderblom, L.A., 1982. The geology of Europa. In: Morrison, D. (Ed.), The Satellites of Jupiter. University of Arizona Press, pp. 521–555.
Marshall, S.T., Kattenhorn, S.A., 2004. Analysis of Europan cycloid morphology and implications for formation mechanisms. In: Workshop on Europa's Icy Shell: Past, Present, and Future. LPI Contribution No. 1195, Lunar and Planetary Institute, Houston, pp. 49–50.
Marshall, S.T., Kattenhorn, S.A., 2005. A revised model for cycloid growth mechanics on Europa: evidence from surface morphologies and geometries. Icarus 177, 341–366.
Martel, S.J., 1997. Effects of cohesive zones on small faults and implications for secondary fracturing and fault trace geometry. Journal of Structural Geology 19, 835–847.
Martel, S.J., Boger, W., 1998. Geometry and mechanics of secondary fracturing around small three-dimensional faults in granitic rock. Journal of Geophysical Research 103, 21,299–21,314.
McEwen, A.S., 1986. Tidal reorientation and the fracturing of Jupiter's moon Europa. Nature 321, 49–51.
McKinnon, W.B., 1999. Convective instability in Europa's floating ice shell. Geophysical Research Letters 26, 951–954.
Nemat-Nasser, S., Horii, H., 1982. Compression-induced nonplanar crack extension with application to splitting, exfoliation and rockburst. Journal of Geophysical Research 87, 6805–6821.
Nimmo, F., Gaidos, E., 2002. Strike-slip motion and double ridge formation on Europa. Journal of Geophysical Research 107, 1–8.
Ojakangas, G.W., Stevenson, D.J., 1989. Polar wander of an ice shell on Europa. Icarus 81, 242–270.
Pappalardo, R.T., Head, J.W., Sherman, N.D., Greeley, R., Sullivan, R.J., The Galileo Imaging Team, 1998. Classification of Europan ridges and troughs and a possible genetic sequence. Proceedings of the Lunar and Planetary Science Conference 29, 1859.
Pappalardo, R.T., Head, J.W., Greeley, R., et al., 1998. Geological evidence for solid-state convection in Europa's ice shell. Nature 391, 365–368.
Pappalardo, R.T., Belton, M.J.S., Breneman, H.H., et al., 1999. Does Europa have a subsurface ocean? Evaluation of the geological evidence. Journal of Geophysical Research 104, 24,015–24,056.
Petit, J.P., Mattauer, M., 1995. Palaeostress superimposition deduced from mesoscale structures in limestone: the Matelles exposure, Languedoc, France. Journal of Structural Geology 17, 245–256.
Pollard, D.D., 1987. Elementary fracture mechanics applied to the structural interpretation of dykes. In: Halls, H.C., Fahrig, W.F. (Eds.), Mafic Dyke Swarms. Special Paper of the Geological Association of Canada 34, pp. 5–24.
Pollard, D.D., Segall, P., 1987. Theoretical displacements and stresses near fractures in rock: with applications to faults, joints, veins, dikes, and solution surfaces. In: Atkinson, B.K. (Ed.), Fracture Mechanics of Rock. Academic Press, London, pp. 277–349.
Prockter, L.M., Pappalardo, R.T., 2000. Folds on Europa: implications for crustal recycling and accommodation of extension. Science 289, 941–943.
Prockter, L.M., Antman, A., Pappalardo, R.T., Head, J.W., Collins, G.C., The Galileo SSI Team, 1999. Europa: stratigraphy and geologic history of an anti-jovian region from Galileo E14 SSI data. Journal of Geophysical Research 104, 16,531–16,540.
Prockter, L.M., Pappalardo, R.T., Head, J.W., 2000. Strike-slip duplexing on Jupiter's icy moon Europa. Journal of Geophysical Research 105, 9483–9488.
Prockter, L.M., Head, J.W., Pappalardo, R.T., Patel, J.G., Sullivan, R.J., Clifton, A.E., Giese, B., Wagner, R., Neukum, G., 2002. Morphology of Europan bands at high resolution: a mid-ocean ridge-type rift mechanism. Journal of Geophysical Research 107, doi:10.1029/2000JE001458.
Rispoli, R., 1981. Stress fields about strike-slip faults inferred from stylolites and tension gashes. Tectonophysics 75, T29–T36.

Rist, M.A., Jones, S.J., Slade, T.D., 1994. Microcracking and shear fracture in ice. Annals of Glaciology 19, 131–137.

Rubin, A.M., 1993. Tensile fracture of rock at high confining pressure: implications for dike propagation. Journal of Geophysical Research 98, 15,919–15,936.

Sarid, A.R., Greenberg, R., Hoppa, G., Hurford, T.A., Tufts, R., Geissler, P., 2002. Polar wander and surface convergence of Europa's ice shell: evidence from a survey of strike-slip displacement. Icarus 158, 24–41.

Schenk, P., McKinnon, W.B., 1989. Fault offsets and lateral crustal movement on Europa: evidence for a mobile ice shell. Icarus 79, 75–100.

Schenk, P., Pappalardo, R.T., 2002. Stereo and photoclinometric topography of chaos and anarchy on Europa: evidence for diapiric origins. Proceedings of the Lunar and Planetary Science Conference 33, 2035.

Schubert, G., Anderson, J.D., Spohn, T., McKinnon, W.B., 2004. Interior composition, structure and dynamics of the Galilean satellites. In: Bagenal, F., Dowling, T.E., McKinnon, W.B. (Eds.), Jupiter: The Planet, Satellites and Magnetosphere. Cambridge University Press, New York, pp. 281–306.

Schulson, E.M., 2002. On the origin of a wedge crack within the icy crust of Europa. Journal of Geophysical Research 107, 1–9.

Sih, G.C., 1974. Strain–energy–density factor applied to mixed-mode crack problems. International Journal of Fracture 10, 305–321.

Spaun, N.A., Head, J.W., Pappalardo, P.T., The Galileo Imaging Team, 1998. Geologic history, surface morphology and deformation sequence in an area near Conamara Chaos, Europa. Proceedings of the Lunar and Planetary Science Conference 29, 1899.

Spaun, N.A., Head, J.W., Pappalardo, R.T., 2002. The spacing distances of chaos and lenticulae on Europa. Proceedings of the Lunar and Planetary Science Conference 33, 1723.

Spaun, N.A., Pappalardo, R.T., Head, J.W., 2003. Evidence for shear failure in forming near-equatorial lineae on Europa. Journal of Geophysical Research 108, doi:10.1029/2001JE001499.

Sullivan, R., Greeley, R., Homan, K., et al., 1998. Episodic plate separation and fracture infill on the surface of Europa. Nature 391, 371–373.

Tufts, B.R., Greenberg, R., Hoppa, G., Geissler, P., 1999. Astypalaea Linea: a large strike-slip fault on Europa. Icarus 141, 53–64.

Tufts, B.R., Greenberg, R., Hoppa, G., Geissler, P., 2000. Lithospheric dilation on Europa. Icarus 146, 75–97.

Vermilye, J.M., Scholz, C.H., 1998. The process zone: a microstructural view of fault growth. Journal of Geophysical Research 103, 12,223–12,237.

Willemse, E.J.M., Pollard, D.D., 1998. On the orientation and patterns of wing cracks and solution surfaces at the tips of a sliding flaw or fault. Journal of Geophysical Research 103, 2427–2438.

Willemse, E.J.M., Peacock, D.C.P., Aydin, A., 1997. Nucleation and growth of strike-slip faults in limestones from Somerset, U.K. Journal of Structural Geology 19, 1461–1477.

Younes, A., Engelder, T., 1999. Fringe cracks: key structures for the interpretation of progressive Alleghanian deformation of the Appalachian Plateau. GSA Bulletin 111, 219–239.

Zahnle, K.L., Schenk, P., Levison, H., Dones, L., 2003. Cratering rates in the outer solar system. Icarus 163, 263–289.